PUBLISHED ONLINE: 17 NOVEMBER 2014 | DOI: 10.1038/NMAT4125

nature materials

Chiral templating of self-assembling nanostructures by circularly polarized light

Jihyeon Yeom[1], Bongjun Yeom[2], Henry Chan[3], Kyle W. Smith[4], Sergio Dominguez-Medina[4], Joong Hwan Bahng[5], Gongpu Zhao[6], Wei-Shun Chang[4], Sung-Jin Chang[7,8], Andrey Chuvilin[9,10], Dzmitry Melnikau[9,11], Andrey L. Rogach[12], Peijun Zhang[6,13], Stephan Link[4], Petr Král[3,14] and Nicholas A. Kotov[1,2,5]*

The high optical and chemical activity of nanoparticles (NPs) signifies the possibility of converting the spin angular momenta of photons into structural changes in matter. Here, we demonstrate that illumination of dispersions of racemic CdTe NPs with right- (left-)handed circularly polarized light (CPL) induces the formation of right- (left-)handed twisted nanoribbons with an enantiomeric excess exceeding 30%, which is ~10 times higher than that of typical CPL-induced reactions. Linearly polarized light or dark conditions led instead to straight nanoribbons. CPL 'templating' of NP assemblies is based on the enantio-selective photoactivation of chiral NPs and clusters, followed by their photooxidation and self-assembly into nanoribbons with specific helicity as a result of chirality-sensitive interactions between the NPs. The ability of NPs to retain the polarization information of incident photons should open pathways for the synthesis of chiral photonic materials and allow a better understanding of the origins of biomolecular homochirality.

Materials with nanoscale chirality are known to strongly rotate the polarization of linearly polarized (LinP) and circularly polarized light (CPL). Such optical effects in nanomaterials with different chiral geometries are being actively investigated as a part of chiral photonics and plasmonics[1–8]. The opposite effects—that is, the transfer of spin angular momenta of circularly polarized photons to matter and its subsequent nanoscale or atomic restructuring, retaining the 'memory' of circular polarization—are much less known. The possibility of such effects at the atomic and nanometre scale is indicated by, for instance, the formation of spiral nanoneedles with controlled helicity during laser ablation of bulk metallic tantalum with CPL (ref. 9); however, the underlying mechanism is not well understood. The transfer of spin angular momenta in high-intensity laser beams has also been observed for Bose–Einstein condensates[10], ensembles of cold atoms[11] and microscale colloids[12]. These special chromophores/scatterers acquired circular or spiral motion while being illuminated by high-intensity CPL. However, it is difficult to convert the photon spin into permanent structural changes of atomic and particulate systems, owing to their achiral symmetry, structural barriers for channelling the rotational energy into chemical bonds, and fast quenching of rotational motion by the media.

The transfer of spin angular momentum into particle rotation has been observed for a wide range of sizes and molar masses (M) of particles—from $M \approx 10^2$ for ensembles of cold atoms[11] to $M \approx 5 \times 10^{12}$ for microscale colloids[12]. The effects of CPL could be possible to observe for nanoparticles (NPs), which are intermediate in mass and size between atom clusters and microparticles, and are similar in masses to Bose–Einstein condensates ($M \approx 10^7$; ref. 10). NP dispersions stable at ambient conditions are more convenient to use than some of these chromophores/scatterers, and can be more reactive than polymeric colloids[12] or bulk tantalum[9]. Also, the photochemical effects of light with different handedness should be enhanced in NPs because of their larger physical size compared with chiral organic molecules[13,14].

CPL-induced restructuring of NP systems can provide a new, powerful, versatile tool for (nano)chemistry of chiral materials. The interest in the synthesis of chiral nanostructures has been fuelled by the potential application of chiral nanostructures in biosensing, telecommunication, display technologies, diffraction-free patterning and chiral catalysis[2–7]. Further motivation to study long-term structural changes caused by CPL in matter is evidenced by the ongoing discussion about the origin of homochirality in natural compounds. Natural amino acids and sugars exist predominantly as left-handed (LH) and right-handed (RH) enantiomers, respectively. Illumination with CPL (refs 15–17) was recently suggested as one of the plausible causes of homochirality[15–17]. However, the mechanism of how CPL can lead to homochirality of organic molecules is not known. Several chemical routes are being debated[18], including chiral amplification[19].

Self-assembly of NPs is one of the mechanisms that could potentially be influenced by CPL. Such expectations are based on: the atomic and nanoscale chirality of individual NPs (refs 20,21);

[1]Department of Macromolecular Science and Engineering, University of Michigan, Ann Arbor, Michigan 48109, USA. [2]Department of Chemical Engineering, University of Michigan, Ann Arbor, Michigan 48109, USA. [3]Department of Chemistry, University of Illinois at Chicago, Chicago, Illinois 60607, USA. [4]Department of Chemistry, Rice University, Houston, Texas 77005, USA. [5]Department of Biomedical Engineering, University of Michigan, Ann Arbor, Michigan 48109, USA. [6]Department of Structural Biology, University of Pittsburgh School of Medicine, Pittsburgh, Pennsylvania 15260, USA. [7]Division of Material Sciences, Korea Basic Science Institute, Daejeon 305-333, Republic of Korea. [8]Department of Chemistry, Chung-Ang University, 84 Heukseok-ro, Dongjak-gu 156-756, Republic of Korea. [9]CIC NanoGUNE Consolider, Tolosa Hiribidea 76, Donostia-San Sebastian 20018, Spain. [10]Ikerbasque, Basque Foundation for Science, Alameda Urquijo 36-5, 48011 Bilbao, Spain. [11]Centro de Física de Materiales (MPC, CSIC-UPV/EHU), Po Manuel de Lardizabal 5, Donostia-San Sebastian 20018, Spain. [12]Department of Physics and Materials Science and Centre for Functional Photonics (CFP); City University of Hong Kong, 83 Tat Chee Avenue, Kowloon, Hong Kong. [13]Department of Mechanical Engineering and Materials Science, Swanson School of Engineering, University of Pittsburgh, Pittsburgh, Pennsylvania 15260, USA. [14]Department of Physics, University of Illinois at Chicago, Chicago, Illinois 60607, USA. *e-mail: kotov@umich.edu

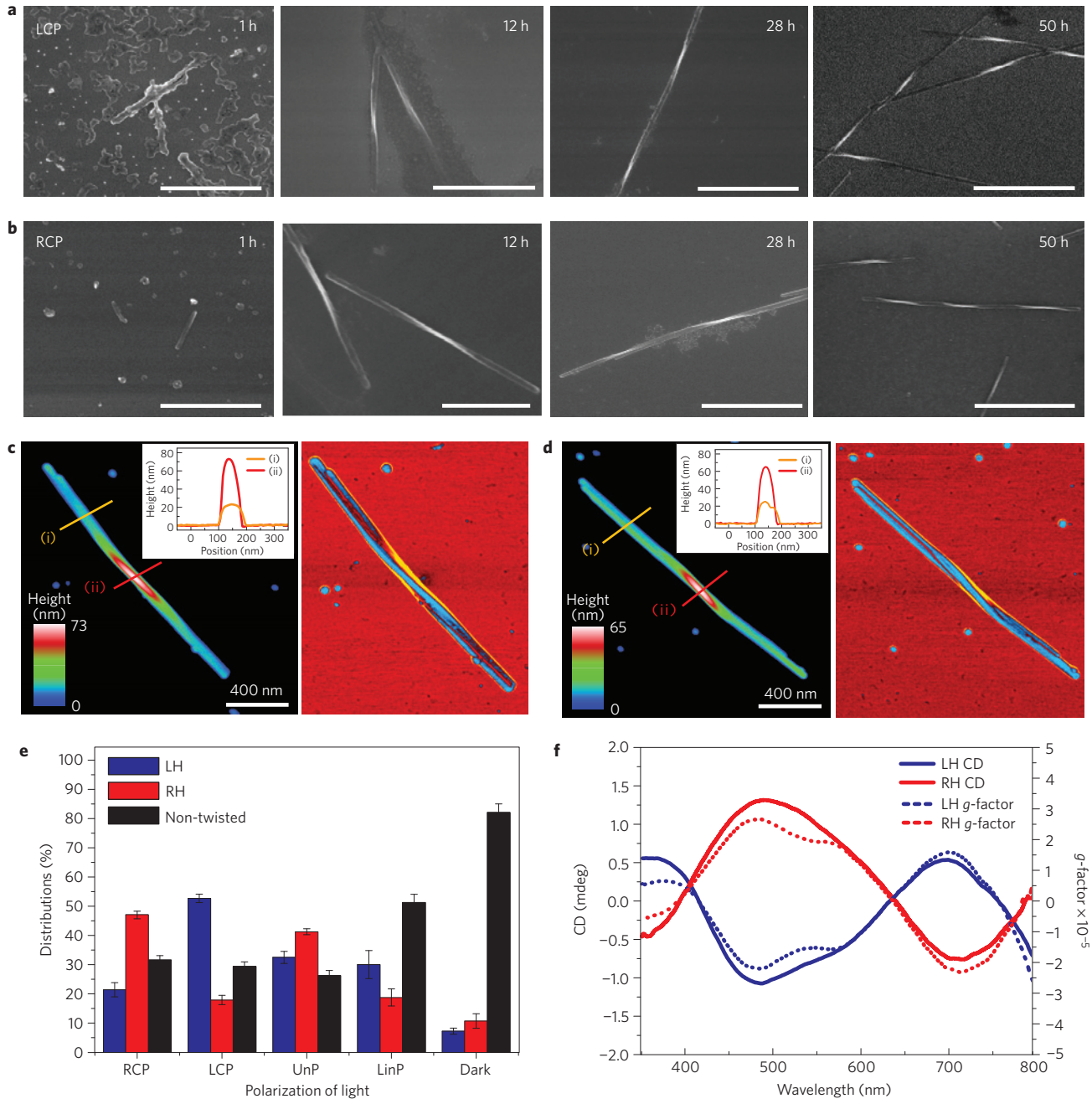

Figure 1 | Self-assembly of CdTe NPs into twisted nanoribbons induced by illumination with CPL. a,b, SEM images of ribbons assembled with LCP (**a**) and RCP (**b**) as a function of time exposure for 1 h, 12 h, 28 h and 50 h. All scale bars are 1 μm. **c,d**, Tapping-mode atomic force microscopy (AFM) topographic (left) and phase (right) images of a LH nanoribbon (**c**) and a RH nanoribbon (**d**). **e**, Distributions of LH, RH and non-twisted nanoribbons obtained after 50 h illumination with RCP, LCP, UnP, LinP light, and in the dark. **f**, Ensemble CD spectra (solid line) and *g*-factor (dotted line) of dispersions of left-handed (LH) nanoribbons and right-handed (RH) nanoribbons obtained after 50 h of CPL illumination. Linear dichroism effects that could be associated with adsorption on the walls of the cuvette and other spontaneous alignment of linear nanostructures have negligible contribution to the chiroptical properties, as indicated by the near identity of the CD spectra obtained with and without stirring of the dispersion.

amplification of circular polarization effects in NP assemblies[22,23]; and the sensitivity of self-assembly processes to small changes in interparticle interactions[24]. Also, inorganic NPs represent a convenient building block for nanoscale synthesis, affording a variety of pathways to develop geometrically complex nanostructures.

Based on this hypothesis, we investigated the effects of CPL on the assembly of water-soluble NPs under ambient conditions. A dispersion of CdTe NPs, stabilized by the achiral capping agent thioglycolic acid (TGA), was illuminated either by left- (LCP) or right-handed circularly polarized (RCP) light with a wavelength of 543 nm. Note that this CdTe dispersion revealed no circular dichroism (CD) peaks in the visible range (Supplementary Fig. 1) and therefore has equal cumulative absorbance for LCP and RCP photons at 543 nm. From a previous study[25], we expected the formation of twisted nanoribbons, but it was unclear whether the polarization of light would have an effect on their assembly pattern and geometry. CPL-induced transformations of NPs were examined after 1, 12, 28, 35 and 50 h of illumination (Fig. 1a,b).

NATURE MATERIALS DOI: 10.1038/NMAT4125

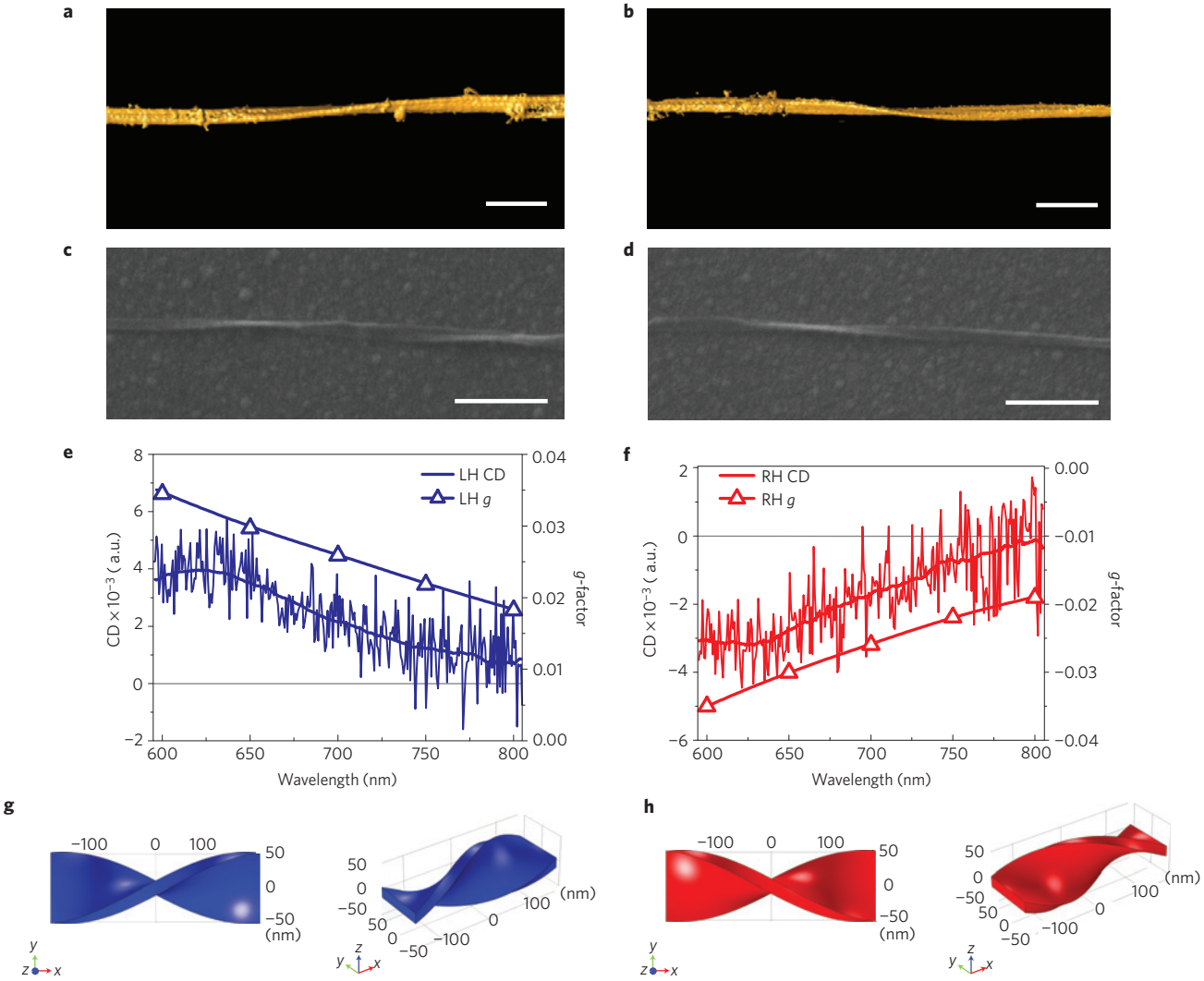

Figure 2 | Chirality of single nanoribbons. a,**b**, Surface rendering of the 3D TEM tomographic reconstruction of a LH (**a**) and a RH (**b**) nanoribbon. Scale bars, 100 nm. See also the Supplementary Movie file for a 3D rendering of the LH nanoribbon. **c**,**d**, SEM images of single LH (**c**) and RH (**d**) nanoribbons. Scale bars, 500 nm. **e**,**f**, CD spectra and calculated *g*-factor spectra for the single LH (**e**) and RH (**f**) nanoribbons in **c**,**d**, respectively. **g**,**h**, Computational models of the LH (**g**) and RH (**h**) nanoribbons used in the FEM calculations of chiroptical properties on the basis of numerical solutions of the Maxwell equations.

The temporal progression of the products included short 50–200 nm rods (1 h) that evolved into 1–2 μm twisted nanoribbons (12 h) and, subsequently, into longer nanoribbons 2–3 μm in length (28 h). After 50 h of illumination, twisted nanoribbons with total lengths, pitch lengths and diameters of 3 ± 0.5 μm, 800 ± 20 nm and 50 ± 5 nm, respectively, were the predominant products of the photoinduced reaction (Fig. 1c,d and Supplementary Information). When nanoribbons were exposed to CPL for more than 96 h, they started to be thinner, but retained their twisted shape (Supplementary Fig. 2). After 50 h of photoinduced assembly, and in the absence of further illumination, the nanoribbons retained their geometry for the entire project time (3.5 years).

Circular polarization of light exhibited an enantio-selective photochemical influence on NP dispersions and on the geometry of the self-assembled nanoribbons. Under LCP illumination, predominantly left-handed (LH) nanoribbons were formed, as established by scanning electron microscopy (SEM) (Fig. 1a and Supplementary Fig. 3). When the NP dispersion was illuminated with RCP, right-handed (RH) nanoribbons of otherwise similar dimensions prevailed (Fig. 1b and Supplementary Fig. 4). In both cases, the differences between LH and RH nanoribbon fractions obtained after analysis of 100 SEM images of ~1,000 nanoribbons were more than 30% (Fig. 1e), which was well in excess of the experimental error of ~5%. Note that this is also much higher than a typical enantiomeric excess in CPL-stimulated organic reactions (0.5–2%; ref. 14). The chiral preference in nanoribbon geometry was also confirmed by CD spectroscopy. CD spectra of purified nanoribbons were measured in aqueous dispersions and revealed distinct chiroptical bands at 490, 590 and 700 nm (Fig. 1f). Comparison of CD and absorption spectra after 50 h illumination (Supplementary Fig. 6) indicates that the first two bands in the CD spectra are associated with the absorption in the bandgap transition. Importantly, nanoribbon dispersions illuminated by LCP and RCP showed positive and negative CD signals, respectively. Transmission electron microscopy (TEM) tomography (Fig. 2a,b), capable of visualizing 3D structures of the nanoribbons, corroborated the conclusions regarding their chiral shape.

A control experiment involving illumination with unpolarized light (UnP) showed an equal distribution between right- and left-handed nanoribbons, in agreement with a previous study[25]. Illumination with LinP as well as incubation in the dark yielded straight nanowires, which were the overwhelmingly dominant

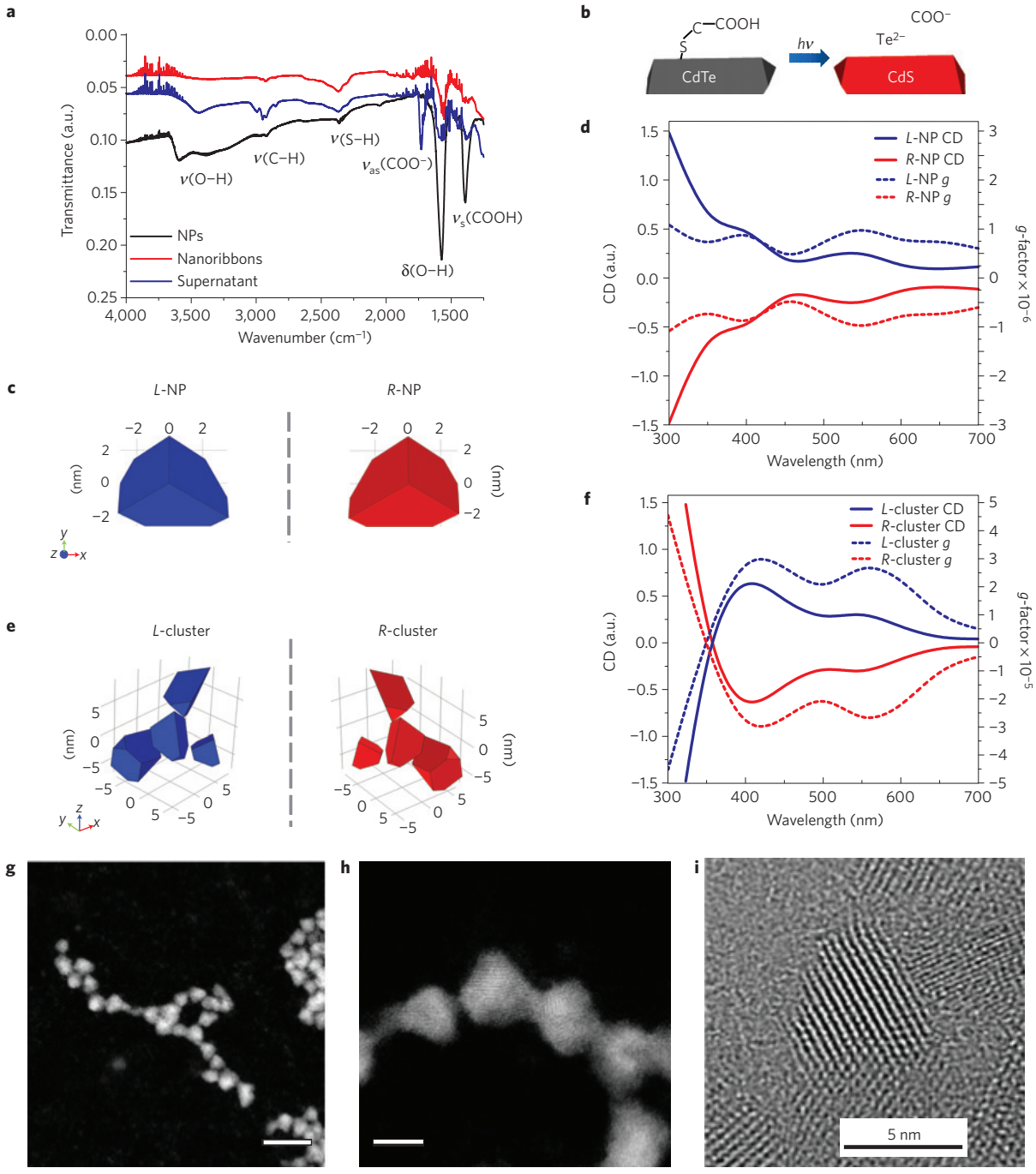

Figure 3 | Mechanism of enantio-selective assembly of NPs. a, FTIR spectra of original CdTe NPs, of the purified nanoribbons and of the supernatant obtained after 50 h of illumination time. **b**, Schematic illustration of the CdTe phase transition to CdS. **c**,**e**, Models of chiral NPs (**c**) and chiral NP clusters (**e**) used in calculations of the chiroptical properties. **d**,**f**, Simulated spectra and *g*-factors for *L*/*R*-NPs (**d**) and *L*/*R*-clusters of NPs (**f**). The nomenclature for NPs and their clusters is based on their positive (*L*) or negative (*R*) optical activity. **g**,**h**, HAADF STEM images of TGA-stabilized truncated tetrahedral CdTe NPs. Scale bars, 15 nm (**g**) and 5 nm (**h**). **i**, High-resolution TEM image of TGA-stabilized truncated tetrahedral CdTe NPs.

products in these two cases. Nanowires produced by exposure to UnP and LinP revealed no CD activity (Supplementary Fig. 7), consistent with the SEM data (Supplementary Fig. 9).

Another experimental series contributing to the understanding of the templating effect of photons on the mesoscale geometry of nanoribbons and nanowires was the illumination of CdTe dispersions with a different light source at 607 nm for 50 h. Compared with illumination at 543 nm, the efficiency of chiral induction by LCP is reduced as the difference between the yield of LH and RH nanoribbons drops to ~20% (Supplementary Fig. 10). This observation is consistent with the reduced intensity of NP absorbance at the fringes of the bandgap transition (Supplementary Fig. 1B).

To avoid the effects of chirality arising from potential artefacts associated with the presence of small molecular weight compounds in solution, we compared CD spectroscopy data of ensembles of chiral structures in dispersion with CD measurements taken for single nanoribbons (Fig. 2e,f) for the 600–800 nm spectral window. The single LH and RH nanoribbons revealed correspondingly positive and negative mirror-image CD signals. A band located

at ~660–700 nm is spectrally similar to the band observed for dispersions (Fig. 1f; the effective spectral window of the quarter-wave plate used prevents single-particle CD measurements in the 400–600 nm region). Supplementary Figs 11 and 12 demonstrate that the CD spectra of the single twisted nanoribbons measured using dark-field microscopy are dominated by light scattering. Therefore, the 'red' CD bands in Fig. 1f should be predominantly attributed to scattering of LCP and RCP photons on twisted nanoribbons with specific handedness and, in fact, may be considered in the framework of circular intensity differential scattering[26]. As a control experiment against potential artefacts we measured CD spectra from single nanoribbons at various rotational angles with respect to the long axis. The shape of the CD spectra remained unchanged regardless of the nanoribbon orientation (Supplementary Fig. 13). As another control experiment, confirming attribution of the origin of the CD bands, non-twisted nanoribbons showed no CD signals (Supplementary Fig. 14).

The chiroptical properties of the twisted nanoribbons can be compared with those of microscale gold helices made by 3D lithography[8], which also exhibit broadband polarization rotation. Anisotropy factors of $g = 0.02$–0.04 were obtained from numerical finite element method (FEM) solutions of the Maxwell equations for CdTe twisted ribbon models (Fig. 2e,f), and are comparable to the values obtained for Ag-enhanced Au nanohelices and Au nanorods/fibre composites, $g \sim 0.025$ (refs 2,3).

To understand how the circular polarization of photons causes distinct permanent differences in the shapes of nanoribbons, we first addressed the mechanism of light-induced self-assembly of CdTe NPs. From the optical properties (Supplementary Fig. 7) and the relative content of NPs in the supernatant of nanoribbon dispersions assembled with and without light (Supplementary Fig. 15), it becomes apparent that, along with the spontaneous self-assembly of NPs (refs 25,27), there is a parallel light-stimulated process of the formation of twisted ribbons. We found that Fourier transform infrared (FTIR) spectroscopy peaks for ν(O–H), δ(O–H) and ν_s(COOH), which are characteristic of the TGA ligand (located at 3,500 cm^{-1}, 1,567 cm^{-1} and 1,421 cm^{-1}, respectively), were drastically decreased for nanoribbons compared to the original CdTe NPs (Fig. 3a). A strong peak at 1,722 cm^{-1}, corresponding to $\nu_{as}(COO^-)$ of carboxyl moieties, was observed in the supernatant obtained after the separation of twisted nanoribbons and NPs by centrifugation. Concomitantly, the characteristic UV–Vis absorption peak of TGA at 276 nm decreased as the illumination time increased (Supplementary Fig. 16), indicating its decomposition. The presence of a S 2*p* signal from CdS in the X-ray photoelectron spectra (XPS) of nanoribbons (Supplementary Fig. 17) and the weakness of peaks for Te from CdTe (Supplementary Fig. 18) indicate that illumination also results in the replacement of Te by S in the NPs; the elemental atomic composition of the nanoribbons was 51.5% Cd, 47.3% S and 1.2% Te (Supplementary Table 1). The mechanism for the photoinduced replacement of Te by S in NPs is likely to involve the ionic diffusion of S^{2-} ions formed by photoinduced oxidation of TGA into the NPs. TEM of the twisted region (Supplementary Figs 19 and 20), atomic mapping images (Supplementary Fig. 22) and energy dispersive spectroscopy (EDS) spectra (Supplementary Figs 23 and 24) confirmed the transformation of CdTe NPs into CdS NPs (Fig. 3b). These results are consistent with previous findings regarding the formation of a thin CdS shell around CdTe NPs due to the chemical decomposition of TGA (Supplementary Information) and the photoinduced oxidation of CdTe (ref. 28).

X-ray photoelectron spectra (Supplementary Fig. 26) indicated that there was no significant difference in the chemical composition of left- and right-handed nanoribbons. Therefore, the assembly mechanism should be the same for RCP and LCP illumination. Spectroscopy and microscopy data in Fig. 3 and Supplementary Figs 16–27 (see Supplementary Information for details) suggest that the mechanism of light-induced nanoribbon self-assembly starts with the photoinduced decomposition of TGA to form S^{2-}, which subsequently replaces Te^{2-} ions in NPs. The loss of the already sparse TGA shell is likely to be the trigger of the light-induced NP assembly into twisted structures. However, such attribution of the self-assembly mechanism encounters an unexpected complication: the electrokinetic zeta potential, ζ, decreased from ~−6 mV to ~−15 mV on illumination (Supplementary Fig. 29); such increase in electrostatic repulsion should hinder the assembly process, contrary to the results observed. Calculations of the pair potentials between the NPs using extended Derjaguin–Landau–Verwey–Overbeek theory (E-DLVO) help to explain this discrepancy and confirm the light-induced assembly mechanism. Even though the zeta potential of 'bare' CdS NPs is more negative, the loss of the TGA shell and increased ionic strength associated with the surface-ligand photooxidation makes the overall pair potential more attractive (Supplementary Fig. 30).

On the basis of the above results, the effect of circular polarization of incident light on NP self-assembly originates in the optically selective activation of nanostructures with different handedness. Both individual CdTe NPs and their clusters can be chiral. As such, aberration-corrected TEM tomography indicates the existence of chiral dislocations of atoms in Pt NPs (ref. 21). Chirality of individual Au NPs in racemic mixtures capped with achiral ligands has been previously shown with liquid chiral chromatography[29]. With the help of high-angle annular dark-field (HAADF) scanning transmission electron microscopy (STEM; Fig. 3g,h), we found that the TGA-stabilized NPs have the shape of a truncated tetrahedron. The distinct truncated tetrahedron shape of CdTe–TGA NPs was also seen in high-resolution TEM images (Fig. 3i). Four uneven truncations result in a chiral tetrahedron similar to a sp^3 hybridized carbon atom with three different substituents (Supplementary Fig. 31). To confirm the chirality of individual NPs, we incubated the dispersion of TGA-stabilized CdTe NPs with bovine serum albumin (BSA, 66.5 kDa), serving here as an enantio-selective absorber. After 5 h of incubation, we separated BSA and unbound NPs using a centrifugal membrane (50 kDa), and measured the CD spectra of the obtained dispersions. In contrast to the original CdTe NPs, which have no CD signals (Supplementary Fig. 1), and BSA, which has a negative CD peak at around 215 nm (Supplementary Fig. 34), the separated NPs showed a positive CD band at 400–550 nm (Supplementary Fig. 35), coinciding with the excitonic transition of the NPs. This observation indicates that the starting NP dispersion is a racemic mixture of NP enantiomers with different chirality that can be enantio-selectively separated.

Simulation of light absorption showed that enantiomers of truncated NPs (Fig. 3c and Supplementary Fig. 31) should exhibit optical activity, as observed in the mirror-imaged simulated CD and *g*-factor spectra (Fig. 3d). Spontaneously formed small clusters of NPs similar to those in Fig. 3g can also be chiral. According to our simulations, the differences in absorption of LCP and RCP in such clusters (Fig. 3f) are even greater than in NPs (Fig. 3d). In both cases, there is a large difference in absorption of LCP and RCP at 543 nm for the nanostructures of different handedness used in this study.

Thus, the mechanism of chirality transfer from CPL to NP assemblies can be understood as follows. The original CdTe NP solution is racemic, containing equal amounts of left- and right-handed particles and small clusters. When a racemic mixture of CdTe NPs (Supplementary Fig. 1A) is illuminated by LCP at 543 nm, a subpopulation of LH NPs and clusters absorb light more effectively (Supplementary Fig. 36, step **2**) than RH NPs and clusters. The same is true for RH NPs/clusters (Supplementary Fig. 36, step **2'**) when the dispersion is illuminated with RCP. The light-activated CdTe NPs undergo photooxidation of the TGA stabilizers; this

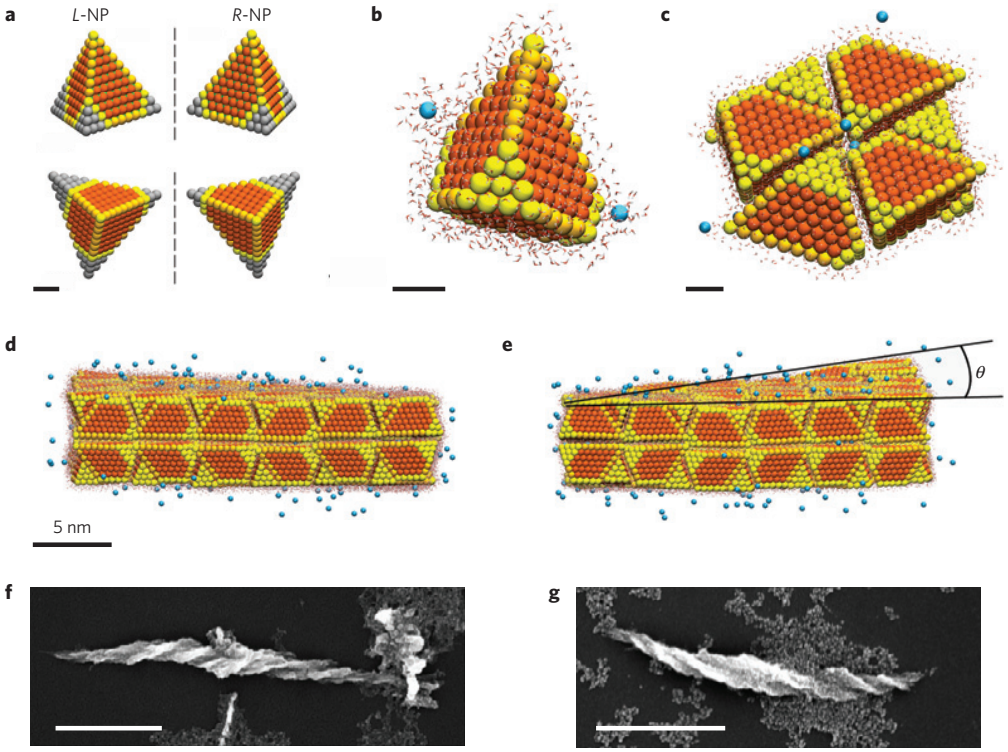

Figure 4 | Molecular dynamics and experimental studies of the self-assembly of chiral NPs. a, Atomistic models of NPs with LH and RH truncations used in MD simulations. **b**, Detailed view of a single NP in an aqueous environment and of the counterions used in the MD simulations. **c**, Fragment of the simulated self-assembled ribbon from a top view, showing the packing of NPs. Scale bars in **a**–**c** are 1 nm. **d**,**e**, Side views of simulated NP ribbons with LH (**d**) and RH (**e**) truncated NPs. The dihedral angle θ determines the pitch of the nanoribbons. **f**,**g**, SEM images of experimental assemblies spontaneously formed in the dark from chiral CdTe NPs stabilized by L-cysteine (**f**) and D-cysteine (**g**). Scale bars, 1 μm.

transforms them into 'bare' CdS NPs. Photooxidation of multiple TGA ligands on the surface of NPs requires multiple photons and, therefore, the difference in the probability of absorption of *L*- and *R*-photons multiplies over time. This process 'locks in' and amplifies the differences between NPs of opposite chirality in the initially racemic mixture.

The ligand-free CdS NPs exhibit a much stronger propensity to self-assemble than ligand-protected, non-light-activated CdTe NPs of opposite handedness (Supplementary Fig. 30). Because the self-assembly of NPs is very sensitive to the anisotropy of NP interactions[27], the chirality of the constituent building blocks is reflected in the helicity of the resulting assemblies, as occurs with the self-assembly of organic and biological macromolecules.

Atomistic molecular dynamics (MD) simulations were performed to further clarify the origin of the observed ribbon helicity (see Supplementary Information for details). Individual NPs were modelled as slightly smaller 3.6 nm tetrahedrons with a cubic CdS crystal lattice and a lattice constant of $a = 0.582$ nm (Fig. 4a). The tetrahedrons were asymmetrically truncated by the removal of 2-, 3- and 4-atom layers from three of the NP vertices to acquire a left or right chirality. The NP surfaces were not coated with stabilizers, in accordance with the experimental results presented in Fig. 3 and Supplementary Figs 16–27, indicating ligand removal in the process of photoactivation. However, the large CdS lattice polarity was reduced at the NP surfaces to one half of the vacuum value to account for the potential presence of residual ligands. NPs at different (homogeneous) charging states were simulated in accordance with experimental observations. The MD simulations were carried out with explicit water molecules and Cl^- counterions of the charged NPs (Fig. 4b and Supplementary Information) to precisely describe the solvent environment of the NP self-assembly process.

Initially, NPs of the same (*L* or *R*) handedness (Fig. 4a) were preassembled into a planar piece of nanoribbon (Fig. 4c) with a packing similar to that observed before[25], assuming that NPs of predominantly one handedness were prepared by photoexcitation with circularly polarized light and self-assembled. On equilibration of the NP assemblies in an isothermal–isobaric ensemble at $T = 300$ K for ~5–10 ns, the planar nanoribbons acquired distinct twists. Importantly, the twist was opposite for NPs with opposite handedness. The average twist angle observed in the simulation of the nanoribbons made from CdS NPs was −3.1° and +4.3° for LH and RH NPs (Fig. 4d,e), respectively, which corresponds to a pitch length of ~1,400–1,900 nm, similar to the experimental pitch length of nanoribbons observed after 28 h illumination in Figs 1 and 2.

These observations confirm the significance of NP chirality in guiding ribbon assembly and the realism of photon–matter chirality transfer via the geometry-specific photoactivation of NPs. The MD simulations indicate that the chirality of the individual NPs translates into a twist of the nanoribbons as a result of cooperative interactions with the NP ensemble. Besides unequal truncations, this phenomenon may be associated with other chiral geometries and multiple inteparticle interactions. Water molecules facilitate this process in all these cases by forming a soft 'cushion' layer between NPs, enabling their restricted mobility. Translation and reorientation of NPs creates the possibility of ensemble-energy minimization in accordance with the chiral bias. The experimental structures are partially disordered (Supplementary Fig. 20), owing to fluctuations in NP size, which translate into some variability of the pitch and of the non-close packing of the NP lattice in the ribbon.

A vivid experimental demonstration of subtle differences in interparticle interactions between a priori chiral NPs leading to nanostructures with different chirality can be obtained for NPs with a stabilizing ligand made from D- and L-cysteine (Fig. 4f,g).

These originally chiral NPs were self-assembled in the dark, and produced submicron helices with distinctly different twist directions depending on the chirality of the building blocks.

In conclusion, we have demonstrated that circular polarization of light can strongly influence assembly of nanoscale structures by altering the chirality of NPs participating in the self-assembly process. Because light sensitivity is common in NPs (see Supplementary Information for details), this study offers new methods of synthesis for chiral nanostructures using light as the primary chiral bias determining the asymmetry in the enantiomeric mixture of the products. Notably, the resulting structures exhibit hierarchical chirality across different scales—molecular, nanoscale and mesoscale—reminiscent of the propagation of chiral asymmetry in biological assemblies. Furthermore, astronomical data indicate that mesoscale and nanoscale particles are present in space[17], whereas geologic records suggest that inorganic NPs were present in primordial Earth conditions[30]; therefore, selective photonic activation of seemingly achiral NPs might have played a role in the origin of homochirality on Earth. This role can be associated with a large variety of catalytic, optical and colloidal processes possible for semiconductor and other nanoparticles under stellar and planetary conditions. At the moment it is premature to speculate about it in greater details. Large enantiomeric excesses observed for CPL-induced NP assemblies (Fig. 1e), exceeding those of known photoinduced reactions in simple organic molecules, merit further studies. Facilitation of the transition of chiral prebiotic structures with preset enantiomeric excess from the molecular scale of early amines, aminoacids, thiols and so on, to the nanometre scale of early biopolymers or organelles may also be considered.

Received 15 August 2014; accepted 2 October 2014; published online 17 November 2014

References

1. Ren, M. X., Plum, E., Xu, J. J. & Zheludev, N. I. Giant nonlinear optical activity in a plasmonic metamaterial. *Nature Commun.* **3,** 833 (2012).
2. Kuzyk, A. *et al.* DNA-based self-assembly of chiral plasmonic nanostructures with tailored optical response. *Nature* **483,** 311–314 (2012).
3. Guerrero-Martinez, A. *et al.* Intense optical activity from three-dimensional chiral ordering of plasmonic nanoantennas. *Angew. Chem. Int. Ed.* **50,** 5499–5503 (2011).
4. Liu, S. *et al.* Synthesis of chiral TiO_2 nanofibre with electron transition-based optical activity. *Nature Commun.* **3,** 1215 (2012).
5. Chen, W. *et al.* Nanoparticle superstructures made by polymerase chain reaction: Collective interactions of nanoparticles and a new principle for chiral materials. *Nano Lett.* **9,** 2153–2159 (2009).
6. Mark, A. G., Gibbs, J. G., Lee, T. C. & Fischer, P. Hybrid nanocolloids with programmed three-dimensional shape and material composition. *Nature Mater.* **12,** 802–807 (2013).
7. Ma, W. *et al.* Attomolar DNA detection with chiral nanorod assemblies. *Nature Commun.* **4,** 2689 (2013).
8. Gansel, J. K. *et al.* Gold helix photonic metamaterial as broadband circular polarizer. *Science* **325,** 1513–1515 (2009).
9. Toyoda, K., Miyamoto, K., Aoki, N., Morita, R. & Omatsu, T. Using optical vortex to control the chirality of twisted metal nanostructures. *Nano Lett.* **12,** 3645–3649 (2012).
10. Brachmann, J. F. S., Bakr, W. S., Gillen, J., Peng, A. & Greiner, M. Inducing vortices in a Bose–Einstein condensate using holographically produced light beams. *Opt. Express* **19,** 12984–12991 (2011).
11. Tabosa, J. W. R. & Petrov, D. V. Optical pumping of orbital angular momentum of light in cold cesium atoms. *Phys. Rev. Lett.* **83,** 4967–4970 (1999).
12. Padgett, M. & Bowman, R. Tweezers with a twist. *Nature Photon.* **5,** 343–348 (2011).
13. Tang, Y. Q. & Cohen, A. E. Enhanced enantioselectivity in excitation of chiral molecules by superchiral light. *Science* **332,** 333–336 (2011).
14. Feringa, B. L. & van Delden, R. A. Absolute asymmetric synthesis: The origin, control, and amplification of chirality. *Angew. Chem. Int. Ed.* **38,** 3419–3438 (1999).
15. Green, M. M. & Selinger, J. V. Cosmic chirality. *Science* **282,** 880–881 (1998).
16. Bailey, J. *et al.* Circular polarization in star-formation regions: Implications for biomolecular homochirality. *Science* **281,** 672–674 (1998).
17. Girl, C. *et al.* Synthesis and chirality of amino acids under interstellar conditions *Top. Curr. Chem* **333,** 41–82 (2013).
18. Cronin, J. R. & Pizzarello, S. Enantiomeric excesses in meteoritic amino acids. *Science* **275,** 951–955 (1997).
19. Prins, L. J., Timmerman, P. & Reinhoudt, D. N. Amplification of chirality: The "sergeants and soldiers" principle applied to dynamic hydrogen-bonded assemblies. *J. Am. Chem. Soc.* **123,** 10153–10163 (2001).
20. Gautier, C. & Burgi, T. Chiral *N*-isobutyryl-cysteine protected gold nanoparticles: Preparation, size selection, and optical activity in the UV–vis and infrared. *J. Am. Chem. Soc.* **128,** 11079–11087 (2006).
21. Chen, C. C. *et al.* Three-dimensional imaging of dislocations in a nanoparticle at atomic resolution. *Nature* **496,** 74–77 (2013).
22. Govorov, A. O., Fan, Z. Y., Hernandez, P., Slocik, J. M. & Naik, R. R. Theory of circular dichroism of nanomaterials comprising chiral molecules and nanocrystals: Plasmon enhancement, dipole interactions, and dielectric effects. *Nano Lett.* **10,** 1374–1382 (2010).
23. Ben Moshe, A., Szwarcman, D. & Markovich, G. Size dependence of chiroptical activity in colloidal quantum dots. *ACS Nano* **5,** 9034–9043 (2011).
24. Talapin, D. V. *et al.* Quasicrystalline order in self-assembled binary nanoparticle superlattices. *Nature* **461,** 964–967 (2009).
25. Srivastava, S. *et al.* Light-controlled self-assembly of semiconductor nanoparticles into twisted ribbons. *Science* **327,** 1355–1359 (2010).
26. Bustamante, C., Maestre, M. F. & Tinoco, I. Circular intensity differential scattering of light by helical structures. 1. Theory. *J. Chem. Phys.* **73,** 4273–4281 (1980).
27. Tang, Z. Y., Kotov, N. A. & Giersig, M. Spontaneous organization of single CdTe nanoparticles into luminescent nanowires. *Science* **297,** 237–240 (2002).
28. Gaponik, N. *et al.* Thiol-capping of CdTe nanocrystals: An alternative to organometallic synthetic routes. *J. Phys. Chem. B* **106,** 7177–7185 (2002).
29. Dolamic, I., Knoppe, S., Dass, A. & Burgi, T. First enantioseparation and circular dichroism spectra of Au_{38} clusters protected by achiral ligands. *Nature Commun.* **3,** 798 (2012).
30. Hartland, A., Lead, J. R., Slaveykova, V. I., O'Carroll, D. & Valsami-Jones, E. The environmental significance of natural nanoparticles. *Nature Educ. Knowl.* **4,** 7 (2013).

Acknowledgements

This material is based on work partially supported by the Center for Solar and Thermal Energy Conversion, an Energy Frontier Research Center funded by the US Department of Energy, Office of Science, Office of Basic Energy Sciences under award number #DE-SC0000957, and by ARO MURI W911NF-12-1-0407 'Coherent Effects in Hybrid Nanostructures for Lineshape Engineering of Electromagnetic Media' (N.A.K. and S.L.). We acknowledge support from the NSF under grant ECS-0601345; CBET 0933384; CBET 0932823; and CBET 1036672. Financial support from the Robert A. Welch Foundation (C-1664) is also acknowledged (S.L.). Support from the NIH grant GM085043 (P.Z.) is gratefully acknowledged. The work of P.K. was supported by the NSF DMR grant No. 1309765 and by the ACS PRF grant No. 53062-ND6. The authors thank J-Y. Kim for assistance with chiral NP assembly experiments.

Author contributions

N.A.K. conceived the project. J.Y. built the experimental set-up and performed the experiments. B.Y. carried out ME-FEM simulations. H.C. and P.K. undertook atomistic MD simulations. K.W.S., S.D-M., W-S.C. and S.L. measured CD signals from a single nanoribbon. J.H.B. conducted E-DLVO calculations and synthesis of L- and D-cysteine-stabilized CdTe nanostructures. G.Z. and P.Z. carried out 3D TEM tomography. S-J.C. conducted AFM measurements. A.C., D.M. and A.L.R. measured high-resolution HAADF and TEM images of truncated tetrahedral CdTe NPs. J.Y., B.Y. and N.A.K. analysed data. J.Y. and N.A.K. wrote the manuscript.

Additional information

Supplementary information is available in the online version of the paper. Reprints and permissions information is available online at www.nature.com/reprints. Correspondence and requests for materials should be addressed to N.A.K.

Competing financial interests

The authors declare no competing financial interests.